Virtual Casing Principle in Presence of Sink/Source Currents

N. Isernia [1], R. Sparago [2,3], F. J. Artola [3], M. Hoelzl [2], G. Rubinacci [1], N. Schwarz [3], S. Ventre [4], and F. Villone [1]

[1]Universitá degli Studi di Napoli Federico II, 80125 Naples, Italy
[2]Max Planck Institute for Plasma Physics, 85748 Garching bei München, Germany
[3]ITER Organization, 13067 St. Paul Lez Durance Cedex, France
[4]Universitá degli Studi di Cassino e del Lazio Meridionale, 03043 Cassino, Italy

The possibility of describing the magnetic field due to currents within a finite control volume via an equivalent surface current distribution on the boundary of such a volume is given by the well-known Virtual Casing Principle (VCP). This has been illustrated and implemented in the past for the case of solenoidal currents in the volume of interest, i.e., when the currents to represent have a null normal component to the boundary of the control volume. Here, we illustrate how to apply and implement the VCP for the more general case where the currents to represent can cross the boundary.

Index Terms— **Boundary conditions, eddy currents, integral equations.**

I. Introduction

THE Virtual Casing Principle (VCP) is a basic corollary of Maxwell's equations in their magneto-quasi-static limit [1], [2], [3]. Consider a region of space V and enclose it by a virtual casing (VC) made of a perfectly conducting material. Then, any current variation within V will generate a surface current in the VC, which prevents any magnetic field variation outside of it. If we are able to calculate the VC surface current distribution, we can use it to calculate the magnetic field in any point outside V, up to the VC itself, via simple Biot–Savart surface integrals.

Shafranov and Zakharov [1] introduced this idea, considering a VC at a closed magnetic flux surface (i.e., a closed surface where $\mathbf{B}\cdot\hat{\mathbf{n}} = 0$). In this case, by simple considerations on the discontinuity of the magnetic field, it is simple to prove that $\mathbf{j}_{\mathrm{VC}} = \mathbf{B} \times \hat{\mathbf{n}}$. The idea was of course not new. Already in the classic textbook of Stratton [4], the magnetic field due to a current source in a domain V was shown to be reproduced outside of the domain by a surface current distribution $\mathbf{B} \times \mathbf{n}/\mu_0$ and a surface distribution of magnetic dipole moment $\mathbf{A} \times \hat{\mathbf{n}}/\mu_0$ exactly at the boundary of V. The latter contribution to the magnetic field is zero exactly when $\mathbf{B} \cdot \hat{\mathbf{n}} = 0$, reproducing Shafranov's idea from a completely different standpoint.

The VC current can be calculated anyway at arbitrary closed surfaces, usually from the magnetic vector potential at the casing itself, leveraging on the solution of a proper boundary integral equation. In Section II, we shall come back to the details and specific hypotheses behind this statement. Given the VC current, the magnetic field is easily calculated via Biot–Savart surface integrals. These properties led to the development of VCP-based "indirect" boundary element method (BEM) models, especially in the magnetic confinement fusion community [5], [6], [7], [8], [9]. These are perfectly equivalent to standard "direct" ones, which are usually implemented to provide an $\mathbf{A} \mapsto \mathbf{B}$ map at the boundary of the domain, in order to provide the correct magnetic boundary conditions to a finite element method (FEM) magneto-quasi-static model of the system inside the domain [10], [11], [12].

The BEM models described above have usually been developed under the hypothesis that the current in the domain under study cannot cross its boundary. A general property was observed by Durand [13], which correctly pointed out that a current crossing the domain boundary should be related to a surface-divergence of the tangential magnetic field, i.e., $\mathrm{div}_S(\mathbf{B} \times \hat{\mathbf{n}}) = \mathbf{j} \cdot \hat{\mathbf{n}}$. Anyway, the problem of efficiently determining the VC current was not discussed in this case.

In the context of magnetically confined fusion plasmas, the coupling of a plasma inside a defined domain with conducting structures outside the domain is an essential simulation problem to be addressed, since the plasma dynamics are directly influenced by the presence of such conducting structures [14], [15], [16]. The electromagnetic forces acting onto these structures can be a substantial engineering concern [17], [18] for which no generally accepted predictive capabilities exist at present, due to the presence of currents shared between plasmas and surrounding conductors (the so-called halo currents) [19], [20], [21], [22]. This circumstance calls for the development of FEM-BEM methods which are capable to handle current distributions which can cross the boundary of the domain [9].

In this article, we describe how a standard VCP-based boundary element method can handle a current crossing the domain boundary. The adaptation of other BEM methods to this situation will be the subject of future work. The article is organized as follows. Section II discusses how to apply the VCP when the current density crosses the VC, and proposes a numerical approximation of the problem. Section III introduces a simple example with analytical solution, used as a

Received 19 July 2025; revised 18 September 2025; accepted 5 October 2025. Date of publication 15 October 2025; date of current version 13 July 2026. Corresponding author: N. Isernia (e-mail: nicola.isernia@unina.it).

Color versions of one or more figures in this article are available at https://doi.org/10.1109/TMAG.2025.3621256.

Digital Object Identifier 10.1109/TMAG.2025.3621256

benchmark. Section IV compares the expected computational costs of different strategies for solving the numerical problem. Section V illustrates application of the method to a more complex 3-D case. Finally, we draw the conclusions in Section VI.

II. Formulation

Consider an arbitrary domain V_{in} containing a current source $\mathbf{j}_{\text{in}}$. This could be the domain of some FEM model in the future. We want to represent the magnetic field generated by $\mathbf{j}_{\text{in}}$ outside V_{in} via an equivalent current distribution at the boundary ∂V_{in} of the domain. Again, we imagine the boundary of the domain to be a VC of perfectly conducting material. Turning on the current source within the control domain V_{in}, a surface current immediately appears on the VC which cancels any induced *electric field* in the VC itself, and hence in the outer domain. The electric field in the outer conductors is related both to the electric scalar potential ϕ and to the magnetic vector potential $\mathbf{a}$, i.e., the condition of zero electric field on the VC reads: $\mathbf{E} = -\partial \mathbf{a}/\partial t - \nabla\phi = 0$. Using the Coulomb gauge, the magnetic vector potential due to different current source contributions is easily found via the Biot–Savart law, i.e., via the operator

$$\mathcal{A} : \mathbf{j}_\alpha \mapsto \frac{\mu_0}{4\pi}\int_\alpha \frac{\mathbf{j}_\alpha(x')}{|x - x'|}\,\mathrm{d}x'. \tag{1}$$

Here, we indicated by $\mathbf{j}_\alpha$ a current density distribution with compact support in α, here either $\alpha =$ in or $\alpha =$ VC. Clearly $\mathbf{a}_\alpha = \mathcal{A}\mathbf{j}_\alpha$. Let us indicate by Σ the contact region between the internal current distribution and the VC, where we allow $\mathbf{j}_{\text{in}} \cdot \hat{\mathbf{n}} = 0$. The interior current density distribution should satisfy three constraints as follows.

1) It needs to be divergence free ($\mathrm{div}\mathbf{j}_{\text{in}} = 0$).
2) It shall not cross the boundary, except at the specified locations ($\mathbf{j}_{\text{in}} \cdot \hat{\mathbf{n}} = 0$ on $\partial V_{\text{in}} \setminus \Sigma$).
3) It cannot determine any global charge accumulation ($\int_{+\partial V_{\text{in}}} \mathbf{j}_{\text{in}} \cdot \hat{\mathbf{n}}\,\mathrm{d}S = 0$).

A correct choice consists in taking $\mathbf{j}_{\text{in}} \in H_L(V_{\text{in}}, \Sigma)$, see [25] for further details. Anyway, we will consider the interior current as assigned in the following, and it is more important here to look at the singular current distribution $\mathbf{j}_{\text{VC}}$, which shall satisfy the following requirements.

1) It shall be always tangent to ∂V_{in}.
2) Its surface divergence should be zero where there is no contact with other current-carrying domains ($\mathrm{div}_S(\mathbf{j}_{\text{VC}}) = 0$ in $\partial V_{\text{in}} \setminus \Sigma$).
3) It cannot determine a global charge accumulation ($\int_{+\partial V_{\text{in}}} \mathrm{div}_S(\mathbf{j}_{\text{VC}})\,\mathrm{d}S = 0$).

In particular, the surface divergence of the VC current shall exactly compensate for the interior current distribution crossing Σ. Finally, the resulting system of integro-differential equations is

$$\mathcal{A}\mathbf{j}_{\text{VC}} + \nabla\chi = -\mathbf{a}_{\text{in}} \quad \text{on } \partial V_{\text{in}} \tag{2}$$

$$\nabla_S \cdot \mathbf{j}_{\text{VC}} = J_n \quad \text{on } \partial V_{\text{in}} \tag{3}$$

where the quantities on the right-hand side represent the magnetic vector potential generated by the internal current distribution, denoted as $\mathbf{a}_{\text{in}}$, and the normal component of the internal current distribution across the VC, indicated as J_n. Clearly, $J_n = 0$ outside of the contact area Σ. Here, the unknown terms are the VC surface current density $\mathbf{j}_{\text{VC}}$ and the time integral of the electric scalar potential $\chi(x,t) = \int \phi(x,\tau)\,\mathrm{d}\tau$. When (2) and (3) are satisfied, the time-integrated voltage measured across any closed field line in the outer domain is certainly zero, up to the VC itself. Hence, we can take any infinitesimally small closed line on the VC, and conclude that $\mathbf{B}\cdot\hat{\mathbf{n}} = 0$ on ∂V_{in}. Simultaneously, the solenoidality constraint on the overall current density guarantees, thanks to Ampère's law, that $\oint_\gamma \mathbf{B}\cdot\hat{\mathbf{t}}\,\mathrm{d}\ell = 0\ \forall$ closed curve γ, even the ones representative of domain handles. The former conditions are sufficient to conclude that $\mathbf{B} = 0$ in the outer domain. Hence, the equivalent current on ∂V_{in} which reproduces exactly the magnetic field due to internal currents in the outer world is clearly $\mathbf{j}_{\text{eq}} = -\mathbf{j}_{\text{VC}}$.

The interest clearly is to solve the VC current problem (2) and (3) numerically. In particular, we properly discretize the VC, e.g., approximating it via straight rectangles or triangles, and choose a finite subspace for the solution space. The basis functions $\mathbf{w}_k$ configuring the approximation subspace are chosen here to have null surface divergence at the locations where there is no current injection ($\mathrm{div}_S\mathbf{w}_k = 0$ on $\partial V_{\text{in}} \setminus \Sigma$) and in such a way that each basis function respects the constraint $\int_{\partial V_{\text{in}}} \mathrm{div}_S\mathbf{w}_k\,\mathrm{d}S = 0$. We accomplish this by providing a negligibly small thickness to the VC and using the basis functions described in [23], which are obtained as the curl of edge shape functions. For representing the electric potential, we introduce one basis function λ_k for each facet discretizing the contact region Σ. The function λ_k is unitary on the facet Σ_k, also defined as *electrode* in the following, and null elsewhere [24]. We indicate by n_e the overall number of electrodes discretizing Σ. The weak form of (2) against the basis functions $\mathbf{w}_k$, together with the weak form of (3) against piecewise constant basis functions λ_k yields the numerical approximation of the problem

$$\mathbf{L}\mathbf{i}_{\text{eq}} + \mathbf{F}\chi_{\text{eq}} = \mathbf{\Phi} \tag{4}$$

$$\mathbf{F}^T\mathbf{i}_{\text{eq}} = \mathbf{J}. \tag{5}$$

Here, we have indicated by $\mathbf{i}_{\text{eq}}$ the unknown degrees of freedom associated with the equivalent currents and by χ_{eq} the corresponding time-integrated potentials on the electrodes of the VC. The forcing term $\mathbf{\Phi}$ in (4) is given by projections of the magnetic vector potentials due to currents within the control volume on the basis functions for the VC, i.e., $\Phi_i = \langle \mathbf{a}_{\text{in}}, \mathbf{w}_i\rangle_{\text{VC}}$. The projection operator is inherited by the scalar product between vector fields in $L^2(\partial V_{\text{in}})$

$$\langle \mathbf{v}, \mathbf{w}\rangle = \int_{\text{VC}} \mathbf{v}\cdot\mathbf{w}\,\mathrm{d}S. \tag{6}$$

The currents injected into the equipotential electrodes are stored in the array $\mathbf{J}$ of (5), i.e., $J_i = -\langle J_n, \lambda_i\rangle_{\text{VC}}$. Clearly, the inductance matrix coefficients are defined by $L_{ij} = \langle \mathcal{A}\mathbf{w}_i, \mathbf{w}_j\rangle_{\text{VC}}$. The *reduced* Kirchhoff incidence matrix for electrodes is calculated as $F_{ij} = \langle \mathbf{w}_i \cdot \hat{\mathbf{n}}, 1\rangle_{\Sigma_j}$. In the *reduced* incidence matrix, we have excluded one electrode from the *complete* incidence matrix, as the associated Kirchhoff current law is linearly dependent on the other $n_e - 1$ [25].

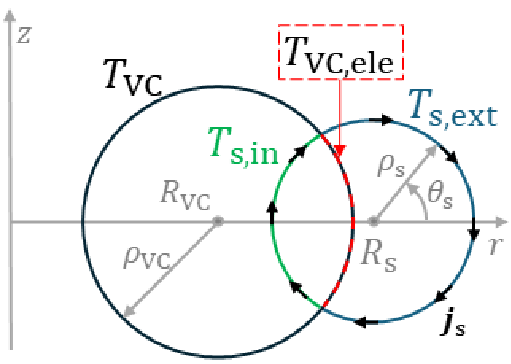

Fig. 1. Trace in the poloidal plane of two intersecting tori: the torus T_s, of major radius R_s and minor radius ρ_s carries a net poloidal current. The exercise consists in replacing the current in $T_{s,\mathrm{in}}$ with an *equivalent* current on the torus T_{VC}, of major radius R_{VC} and minor radius ρ_{VC}.

The solenoidality requirement translates here indeed in $\sum_{k=1}^{n_e} J_k = 0$, which makes apparent that we cannot impose the current in all of the electrodes.

III. Illustrative Example

In this section, we introduce a simple example to provide concrete evidence of the validity of the generalized VCP expressed by (2) and (3). We consider two axisymmetric conducting tori which intersect each other, as depicted in Fig. 1. We assume that both are geometrically thin, and in particular T_s carries a net poloidal current of given value I_s and T_{VC} is our "perfectly conducting" VC. We can subdivide T_s in two distinct portions: $T_{s,\mathrm{in}}$ is the one contained in the volume enclosed by the toroidal VC and $T_{s,\mathrm{ext}}$ is the remainder portion, i.e., the one external respect to T_{VC}. The objective is to find the equivalent current distribution on T_{VC} which perfectly represents the original current distribution on $T_{s,\mathrm{in}}$: the current flowing in $T_{\mathrm{VC}} \cup T_{s,\mathrm{ext}}$ shall produce the same magnetic fluxes and fields everywhere in the region of space external to T_{VC}.

In this axisymmetric context, a poloidal divergence-free current on T_{VC} has only 2 possible degrees of freedom. We choose in particular:

1) I_{net}, associated with the net poloidal current which wraps poloidally around the torus T_{VC} (e.g., in the clockwise direction); and
2) I_{ele}, associated with the clock-wise current along the shortest path on T_{VC} between the intersections lines of the two tori. Let us indicate the portion of the torus affected by this current by the symbol $T_{\mathrm{VC,ele}}$.

Of course, any linear combination of the current distributions described above may be used as a basis for the solution space. With this choice, the d.o.f. I_{ele} is imposed by the current injected from $T_{s,\mathrm{in}}$, i.e., by an equation of the type (5). The determination of the net poloidal current I_{net} is possible via an equation of the type (4). Its set-up and interpretation are particularly intuitive here, since the flux associated with net poloidal current distribution is precisely the net *toroidal flux* linked with the torus T_{VC}. This condition is expressed synthetically by

$$L_{\mathrm{net,net}} I_{\mathrm{net}} + \underbrace{\left(L_{\mathrm{net,ele}} + M_{\mathrm{net,in}}\right)}_{L^*_{\mathrm{net,ele}}} I_{\mathrm{ele}} = 0 \tag{7}$$

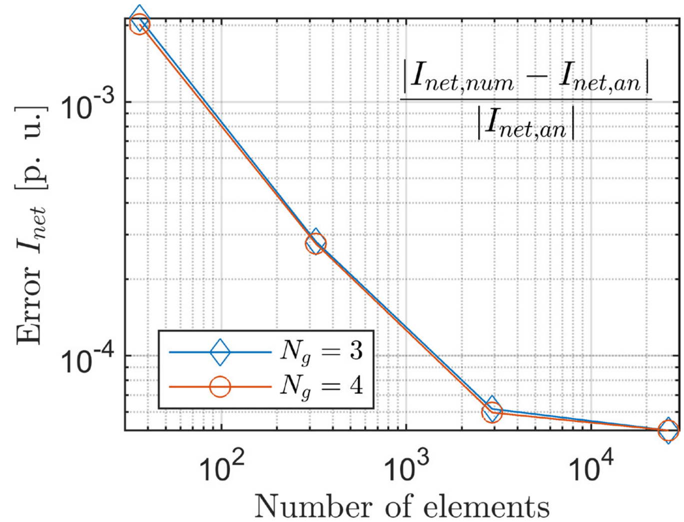

Fig. 2. Resolution scan for the net poloidal VC current of the illustrative example described in Section III. N_g indicates the number of Gauss points per direction and per element used for the integration during the assembly phase of the inductance matrix.

where $L_{\mathrm{net,net}}$ is the inductance of the perfect toroidal solenoid of circular cross section T_{VC}, while $L^*_{\mathrm{net,ele}} = L_{\mathrm{net,ele}} + M_{\mathrm{net,in}}$ also configures the inductance of the perfect toroidal solenoid given by the union of $T_{s,\mathrm{in}} \cup T_{\mathrm{VC,ele}}$. Both can be computed analytically, see the Appendix, hence the net current along T_{VC} can be also computed analytically

$$I_{\mathrm{net}} = -\frac{L^*_{\mathrm{net,ele}}}{L_{\mathrm{net,net}}} I_{\mathrm{ele}}. \tag{8}$$

Notice in particular that in (7) the electrostatic potential does not appear explicitly. This is not a coincidence, as we shall comment in Section IV.

It is worth to notice here that the current distribution associated with I_{net} does not modify in any way the outer magnetic field, since it configures a perfect toroidal solenoid. It is exclusively I_{ele} that contributes to the determination of the magnetic field in the outer domain in this case. This circumstance makes apparent the fact that the VC current shall be determined by imposing the electric field to be null, and that asking the magnetic field to be null would not be sufficient to determine all the current degrees of freedom.

We implement a numerical approximation of the above example via the finite element model described in the previous section. We consider in particular a configuration where $R_{\mathrm{VC}} = 1$ m, $R_s = (1+\sqrt{2})$ m and $\rho_{\mathrm{VC}} = \rho_s = 1$ m. With this choice, the tori intersect orthogonally. We verify that, for increasing resolution, we converge toward the analytical solution proposed. In this numerical exercise, we provide a finite thickness to the current-carrying torus T_s, so that the intersections between the tori are toroidal stripes rather than geometrical lines. While increasing the resolution for the discretization of T_s and T_{VC}, the thickness of T_s is self-consistently reduced, so that we tend to the ideal example. Fig. 2 compares the net poloidal VC current with the analytical result, for different resolution and integration precision levels.

IV. Computational Considerations

We intend here to comment on the best possible way of solving the linear system defined by (4) and (5). There are indeed at least two different possibilities:

1) Exploit the block structure of the linear system to proceed with the inversion. From (4) and (5), the coefficient matrix is indeed

$$\mathbf{M} = \begin{bmatrix} \mathbf{L} & \mathbf{F} \\ \mathbf{F}^T & \mathbf{0} \end{bmatrix}. \tag{9}$$

2) Determine the null space of the electrode-to-current incidence matrix $\mathbf{F}$ and solve separately for the currents which cross electrodes and the currents limited to flow within the VC.

The first strategy relies on using the Schur complement of $\mathbf{L}$ respect to the overall matrix of coefficients $\mathbf{M}$, which is

$$\mathbf{S} = -\mathbf{F}^T\mathbf{L}^{-1}\mathbf{F}. \tag{10}$$

The equivalent current to the one internal to the VC is given by

$$\mathbf{i}_{\text{eq}} = \mathbf{L}^{-1}\{[\mathbf{1} + \mathbf{F}\mathbf{S}^{-1}\mathbf{F}^T\mathbf{L}^{-1}]\mathbf{\Phi} - \mathbf{F}\mathbf{S}^{-1}\mathbf{J}\}. \tag{11}$$

Clearly, the Cholesky factorization of the full symmetric positive definite matrix $\mathbf{L}$ can be performed once, and the forward/backward substitutions applied each time are necessary. A similar consideration applies for the Schur complement $\mathbf{S}$.

The second strategy is based on the decomposition of the solution space for the equivalent current in two distinct subspaces: the sub-space of currents flowing between electrodes, im$\mathbf{F}$, and its orthogonal complement ker$\mathbf{F}'$. It is possible to demonstrate that the whole solution space is given by the direct sum of the above subspaces, see [25] for details. The null space of the sparse incidence matrix $\mathbf{F}'$ can be calculated efficiently, e.g., using sparse algorithms which compute the full QR factorization of the matrix $\mathbf{F}$. The first m columns of the $\mathbf{Q}$ matrix provide by definition an orthogonal base for im$\mathbf{F}$, while the remainder $n-m$ columns span the null space. We collect them into the vector $\mathbf{K}$, so that we can decompose the current in the following way:

$$\mathbf{i}_{\text{eq}} = \mathbf{F}\mathbf{i}_{\text{eq},e} + \mathbf{K}\mathbf{i}_{\text{eq},i}. \tag{12}$$

The currents in im$\mathbf{F}$ are statically determined by the injected currents $\mathbf{J}$

$$\mathbf{i}_{\text{eq},e} = (\mathbf{F}'\mathbf{F})^{-1}\mathbf{J}. \tag{13}$$

Here, the matrix $\mathbf{F}'\mathbf{F}$ is symmetric positive definite and with good sparsity properties, allowing the inversion of (13) to be performed with a number of operations quasi-linear with the number of unknowns. The currents in ker$\mathbf{F}$ can be calculated by projecting (4) on the same subspace, i.e., assembling

$$\mathbf{L}_{ii} = \mathbf{K}'\mathbf{L}\mathbf{K} \tag{14}$$

and solving for the currents

$$\mathbf{i}_{\text{eq},i} = \mathbf{L}_{ii}^{-1}[\mathbf{K}'\mathbf{\Phi} - \mathbf{K}'\mathbf{L}\mathbf{F}\mathbf{i}_{\text{eq},e}]. \tag{15}$$

The determination of currents $\mathbf{i}_{\text{eq},i}$ via (15) does not require information on the electrostatic potential, a feature that has already been observed in (7) for the illustrative example.

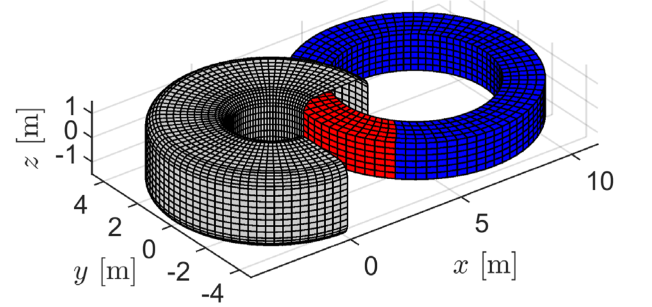

Fig. 3. Geometry for the low resolution test case. A portion of the axisymmetric toroidal surface used for the equivalent current computation is depicted in gray. The portion of the bulk conducting coil contained within the toroidal surface is depicted in red.

Let us analyze the main differences between the two methods, focusing first on the most expensive steps. The first method, based on the idea of the block-inversion, requires to compute the factorization of the inductance matrix L of dimension n and of its Schur complement S of dimension m. The null-based method requires the factorization of the $\mathbf{L}_{ii}$ matrix, of dimension $n-m$ and the solution of the linear system (13) of dimension m. It is already quite clear that the relative performances of the two methods are regulated by the ratio between the number of independent electrodes m and the overall number of current degrees of freedom n. In applications where we allow our VC to deal with a current injection in any point, we expect in particular $m \simeq n/2 \rightarrow (n-m)/n = 1/2$. This means that the factorization of $\mathbf{L}_{ii}$ may eventually cost $\simeq 1/8$ compared to the factorization of the full matrix $\mathbf{L}$. Furthermore, the solution of the sparse symmetric positive definite system (13) can be performed in general much faster than the factorization of the Schur complement S, which has the same dimensions but is fully populated.

Within the potentially expensive matrix-matrix products steps, we have the composition of the Schur complement (10), which requires approximately $nnz(\mathbf{F})n + m^2 n$ operations, where $nnz(\mathbf{F})$ is the number of non-zero entries in the sparse matrix $\mathbf{F}$. With standard libraries, the projection of $\mathbf{L}$ onto the null space defined in (14) requires approximately $nnz(\mathbf{K})n + (n-m)^2 n$ operations. Assuming a similar sparsity both for $\mathbf{F}$ and $\mathbf{K}$, the comparative cost of the operations depends again on the m/n ratio. For $m \ll n$, the block-inversion method could outperform the null-space method during the matrix assembly phase. For the expected ratio of dimension $m/n = 1/2$, these intermediate assembly steps are absolutely comparable, with an overall cost which scales in both cases approximately with $n^3/4$. From the considerations above, we conclude that the approximate costs for the two strategies scale approximately like

$$C_{\text{null}} \simeq k_1 \cdot (n-m)^3 + (n-m)^2 \cdot n \tag{16}$$

$$C_{\text{block}} \simeq k_1 \cdot n^3 + k_1 \cdot m^3 + m^2\, n. \tag{17}$$

For $k_1 = 1/3$, typically assumed for Cholesky factorization, the null strategy should be usually more convenient for $m/n > 0.37$. It is worth noting that if $m \rightarrow n$, the current distribution in the VC is essentially statically determined by the current

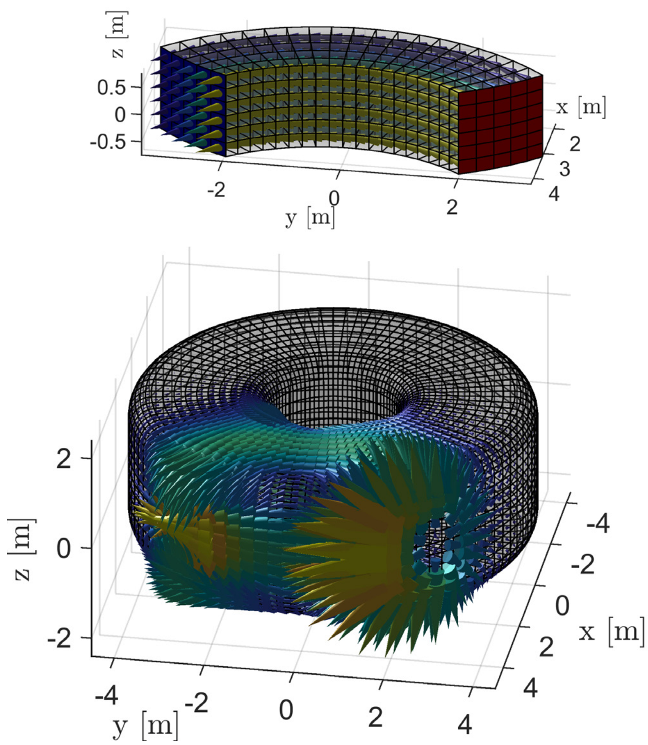

Fig. 4. Top: assigned current density distribution within the toroidal surface. Bottom: corresponding equivalent current distribution.

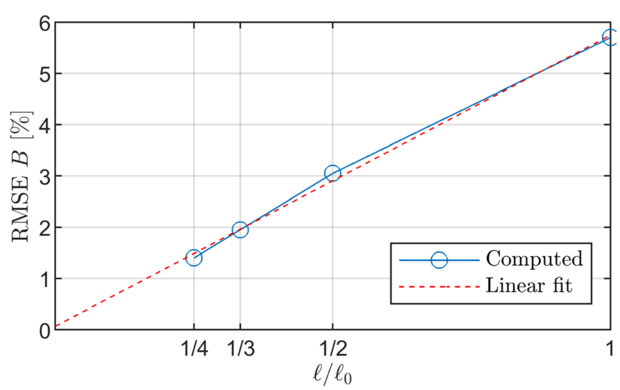

Fig. 5. Scan of magnetic field RMSE with typical linear size of boundary element. The coarsest case $\ell = \ell_0 = 23$ cm corresponds to the equivalent current in Fig. 4.

injection and $C_{\text{null}} \to 0$ in the approximations discussed. This situation may happen in practice if some internal current degrees of freedom are excluded a priori from the model, e.g., because for the class of forcing terms considered, we may know in advance that those will never be solicited.

V. Three-Dimensional Application

A test case for the system of equations (4) and (5) is set up: the geometry and nominal discretization for this toy model are depicted in Fig. 3. A bulk toroidal conductor of rectangular cross section ($R = 3$ m, $\Delta Z = 1.5$ m, and $\Delta R = 1.5$ m) is crossing a toroidal surface of rectangular cross section ($R = 3$ m, $\Delta Z = 3$ m, and $\Delta R = 3$ m), which can represent the boundary of some computational domain in the future. The centers of the two toroids are separated by a distance of 6.5 m along the x-direction.

In the bottom of Fig. 4, we show the equivalent current distribution to the one inside the toroidal surface, shown in the top. This is obtained by inverting the system of (4) and (5).

We compare the magnetic field immediately outside of the VC as generated by our original current distribution and by our equivalent surface current, for different discretization levels. Fig. 5 summarizes the result of the scan, indicating that decreasing the mesh size, the error decreases proportionally.

VI. Conclusion

The VCP is a fundamental equivalence theorem of electromagnetism. The magnetic fields and fluxes due to an arbitrary current distribution $\mathbf{j}_{\text{in}}$ with support in V_{in} can be reproduced, outside of the domain V_{in}, by an equivalent surface current $\mathbf{j}_{\text{eq}}$, flowing on the domain boundary. It was illustrated in the past how to use the VCP to efficiently determine the equivalent current distribution in situations where $\mathbf{j}_{\text{in}}$ was solenoidal in V_{in} (i.e., $\text{div}\mathbf{j}_{\text{in}} = 0\ \forall x \in V_{\text{in}}$, and $\mathbf{j}_{\text{in}} \cdot \hat{\mathbf{n}} = 0\ \forall x \in \partial V_{\text{in}}$). The present contribution significantly expands the possibilities of application of the VCP, by illustrating how to apply it in situations where the source current density distribution $\mathbf{j}_{\text{in}}$ can cross the VC itself, i.e., in situations where $\mathbf{j}_{\text{in}} \cdot \hat{\mathbf{n}}$ can be different from zero at the domain boundary.

The correct system of integro-differential equations to solve, in this more general case, has been given in (2) and (3). A convenient numerical approximation of the problem has been also introduced, leading to the linear algebraic system of (4) and (5). The latter is based on a Finite Element Galerkin method, where the basis functions $\mathbf{w}_k$ for the current density $\mathbf{j}_{\text{eq}}$ are chosen in such a way that: 1) $\nabla_S \cdot \mathbf{w}_k = 0$ at all locations where there is no current crossing the VC, and 2) $\int_{\text{VC}} \nabla_S \cdot \mathbf{w}_k \, dS = 0$. The numerical method was validated using a suitable test case that admits an analytical solution. Furthermore, for a more complex 3-D case, a resolution scan revealed that the magnetic field produced by the equivalent current reproduces the original magnetic field increasingly well as the mesh size decreases.

The most convenient approach for the inversion of the system of equations (4) and (5) has been shown to depend on the number of independent constraints for the current density m, compared to the overall number of degrees of freedom used to represent the equivalent current density n. In particular, a scheme based on the decomposition between the null space of the current density constraints' matrix and its orthogonal complement, could be convenient for $m/n > 0.37$.

Appendix

The self-inductance for a perfect toroidal solenoid is given by

$$L = \frac{\mu_0}{2\pi} \int_{\Omega} \frac{1}{r} \, dS \tag{18}$$

where Ω is an arbitrary poloidal cross section of the toroidal solenoid. For any toroidal solenoid of circular cross section, we may calculate the integrals of interest by defining the shifted radial coordinate $x = r - R$, where R is the major radius of the solenoid. The integral of $1/r$ across the cross section between two arbitrary radially shifted locations x_1 and x_2 is given by

$$\int_{\Omega(x_1,x_2)} 1/r\,\mathrm{d}S = \Bigg[-\sqrt{R^2-\rho^2}\arctan\varphi(x,R,\rho) + R\arctan\frac{x}{\rho^2-x^2} + \sqrt{\rho^2-x^2}\Bigg]_{x_1}^{x_2} = f(x_1,x_2,R,\rho)$$

where

$$\varphi(x,R,\rho) = \frac{\rho^2+Rx}{\sqrt{R^2-\rho^2}\sqrt{\rho^2-x^2}}. \qquad (19)$$

Hence, the self-inductance for the toroidal solenoid T_{VC} of circular cross section Ω_{VC} is given immediately by

$$L_{\mathrm{net,net}} = \frac{\mu_0}{2\pi} f(-\rho_{\mathrm{VC}}, \rho_{\mathrm{VC}}, R_{\mathrm{VC}}, \rho_{\mathrm{VC}}). \qquad (20)$$

Similarly for the case of a toroidal solenoid of lens-shaped cross section, given in our case by the union $T_{s,\mathrm{in}} \cup T_{\mathrm{VC,ele}}$, and whose cross section is given by $\Omega_s \cap \Omega_{\mathrm{VC}}$ is found conveniently by

$$L^*_{\mathrm{net,ele}} = \frac{\mu_0}{2\pi}\big[f(-\rho_s, -d/2, R_s, \rho_s) + f(d/2, \rho_{\mathrm{VC}}, R_{\mathrm{VC}}, \rho_{\mathrm{VC}})\big] \qquad (21)$$

where we indicated the distance between the centers of the tori by $d = R_s - R_{\mathrm{VC}}$.

Acknowledgment

This work was supported by the EUROfusion Consortium by the European Union via the Euratom Research and Training Program under Agreement 101052200. Views and opinions expressed are, however, those of the author(s) only and do not necessarily reflect those of the European Union or the European Commission. Neither the European Union nor the European Commission can be held responsible for them. The research leading to these results has been partially funded by the Project “TRAINER-Tokamak plasmas daTa-dRiven identificAtIon and magNEtic contRol” CUP E53D23014670001 funded by EU in NextGenerationEU plan through the Italian “Bando Prin 2022-D.D. 1409 del 14-09-2022” by Italian University and Research Ministry MUR.

The views and opinions expressed herein do not necessarily reflect those of the ITER Organization.

References

[1] V. D. Shafranov and L. E. Zakharov, “Use of the virtual-casing principle in calculating the containing magnetic field in toroidal plasma systems,” *Nucl. Fusion*, vol. 12, no. 5, pp. 599–601, Sep. 1972.

[2] L. E. Zakharov, “Numerical methods for solving some problems of the theory of plasma equilibrium in toroidal configurations,” *Nucl. Fusion*, vol. 13, no. 4, pp. 595–602, Aug. 1973.

[3] J. D. Hanson, “The virtual-casing principle and Helmholtz’s theorem,” *Plasma Phys. Controlled Fusion*, vol. 57, no. 11, Sep. 2015, Art. no. 115006.

[4] J. A. Stratton, *Electromagnetic Theory*, L. A. DuBridge, Ed., New York, NY, USA: McGraw-Hill, 1941, pp. 250–254.

[5] A. Portone, F. Villone, Y. Liu, R. Albanese, and G. Rubinacci, “Linearly perturbed MHD equilibria and 3D eddy current coupling via the control surface method,” *Plasma Phys. Controlled Fusion*, vol. 50, no. 8, Aug. 2008, Art. no. 085004.

[6] M. Hölzl et al., “Coupling JOREK and STARWALL codes for non-linear resistive-wall simulations,” *J. Phys., Conf. Ser.*, vol. 401, Dec. 2012, Art. no. 012010.

[7] F. Villone, L. Barbato, S. Mastrostefano, and S. Ventre, “Coupling of nonlinear axisymmetric plasma evolution with three-dimensional volumetric conductors,” *Plasma Phys. Controlled Fusion*, vol. 55, no. 9, Sep. 2013, Art. no. 095008.

[8] B. Faugeras and H. Heumann, “FEM-BEM coupling methods for tokamak plasma axisymmetric free-boundary equilibrium computations in unbounded domains,” *J. Comput. Phys.*, vol. 343, pp. 201–216, Aug. 2017.

[9] N. Isernia et al., “Self-consistent coupling of JOREK and CARIDDI: On the electromagnetic interaction of 3D tokamak plasmas with 3D volumetric conductors,” *Phys. Plasmas*, vol. 30, no. 11, Nov. 2023, Art. no. 113901.

[10] F. Brezzi and C. Johnson, “On the coupling of boundary integral and finite element methods,” *Calcolo*, vol. 16, pp. 189–201, May 1979.

[11] C. Johnson and J. C. Nedelec, “On the coupling of boundary integral and finite element methods,” *Math. Comput.,* vol. 35, pp. 1063–1079, Sep. 1980.

[12] A. Bossavit and J.-C. Verite, “A mixed fem-biem method to solve 3-D eddy-current problems,” *IEEE Trans. Magn.*, vol. M-18, no. 2, pp. 431–435, Mar. 1982.

[13] E. Durand, *Magnetostatique*. Paris, France: Masson, 1964, pp. 246–249.

[14] E. A. Lazarus, J. B. Lister, and G. H. Neilson, “Control of the vertical instability in tokamaks,” *Nucl. Fusion*, vol. 30, no. 1, pp. 111–141, Jan. 1990.

[15] D. J. Ward and A. Bondeson, “Stabilization of ideal modes by resistive walls in tokamaks with plasma rotation and its effect on the beta limit,” *Phys. Plasmas*, vol. 2, no. 5, pp. 1570–1580, May 1995.

[16] M. S. Chu and M. Okabayashi, “Stabilization of the external kink and the resistive wall mode,” *Plasma Phys. Controlled Fusion*, vol. 52, no. 12, Dec. 2010, Art. no. 123001.

[17] V. Riccardo, P. Noll, and S. P. Walker, “Forces between plasma, vessel and TF coils during AVDEs at JET,” *Nucl. Fusion*, vol. 40, no. 10, pp. 1805–1810, Oct. 2000.

[18] V. Yanovskiy, N. Isernia, V. D. Pustovitov, and F. Villone, “Sideways forces on asymmetric tokamak walls during plasma disruptions,” *Nucl. Fusion*, vol. 62, no. 8, Aug. 2022, Art. no. 086001.

[19] T. C. Hender et al., “Chapter 3: MHD stability, operational limits and disruptions,” *Nucl. Fusion*, vol. 47, pp. 128–202, Jun. 2007.

[20] J. Adamek et al., “Current density limitation during disruptions due to plasma-sheaths,” *Nucl. Fusion*, vol. 62, no. 8, Jun. 2022, Art. no. 086034.

[21] N. Schwarz et al., “Experiments and non-linear MHD simulations of hot vertical displacement events in ASDEX-upgrade,” *Plasma Phys. Controlled Fusion*, vol. 65, no. 5, Mar. 2023, Art. no. 054003.

[22] N. Schwarz et al., “The mechanism of the global vertical force reduction in disruptions mitigated by massive material injection,” *Nucl. Fusion*, vol. 63, no. 12, Sep. 2023, Art. no. 126016.

[23] R. Albanese and G. Rubinacci, “Finite element methods for the solution of 3D eddy current problems,” *Adv. Imag. Electron Phys.*, vol. 102, pp. 1–86, Mar. 1997.

[24] G. Rubinacci, A. Tamburrino, and F. Villone, “Circuits/fields coupling and multiply connected domains in integral formulations,” *IEEE Trans. Magn.*, vol. 38, no. 2, pp. 581–584, Mar. 2002.

[25] S. Ventre, A. Chiariello, N. Isernia, V. Mottola, and A. Tamburrino, “Modal decomposition in numerical computation of eddy current transients,” 2024, *arXiv:2407.11993*.